DAA/Ames

STATUS REPORT ON NASA GRANT NAG 2-371,

"AN INVESTIGATION OF EMPENNAGE BUFFETING,"

SEPTEMBER 15, 1985 - JANUARY 15, 1986

by

C. Edward Lan and I. G. Lee

January 28, 1986

The Flight Research Laboratory
Department of Aerospace Engineering
The University of Kansas
Lawrence, Kansas 66045

In this report, progress in the investigation of empennage buffeting is reviewed. In summary, the following tasks have been accomplished:

(1) Relevant literatures have been reviewed.

(2) Equations for calculating structural response have been formulated.

(3) Root-mean-square values of root bending moment for a 65-degree rigid delta wing have been calculated and compared with data.

(4) Water-tunnel test program for an F-18 model has been completed.

Items (1) - (3) are described in more detail in Appendix A, while item (4) is presented in Appendix B.

Appendix A:

Investigation of Buffeting by LEX Vortices

by

C. Edward Lan and I. G. Lee

1. INTRODUCTION

Buffeting flow arises when flow separation occurs on an airplane. The resulting flow field is highly turbulent, thus producing fluctuating pressures on lifting surfaces in the detached flow region. Boundary layer separation is perhaps the most common source producing buffet on most conventional configurations. Research in this area has been quite extensive and involved measurements of fluctuating pressures on models together with some theoretical methods to extrapolate these results to full-scale vehicles (see, for example, Refs. 1-3). Frequently, these pressure measurements are made on a conventional "rigid" model, instead of an aeroelastic one, because the latter can not withstand high enough dynamic pressures to be realistic. Based on this consideration, several theoretical methods to use these pressure measurements to predict buffet response have been developed. Some of these methods will be reviewed later. Review of some test results can be found in References 4 and 5; and of theoretical methods, in References 6 and 7.

Of particular interest in the present investigation is the buffeting caused by leading-edge vortices on slender wings. Test results showed that

(a) buffeting was low before vortex breakdown and became severe after that (Ref. 8 and 9);

(b) high-frequency buffeting was caused by boundary layer fluctuation, and leading-edge vortices produced mainly low-frequency fluctuation (Ref. 10);

(c) the results were not sensitive to Reynolds numbers (Refs. 10 and 11), so that flight and tunnel measurements could be well correlated (Ref. 12);

(d) buffeting at vortex breakdown was associated with the wing response at the fundamental mode (Ref. 8).

One conclusion from this early-day research on leading-edge vortces was that the buffeting induced by vortex breakdown would mostly be academic because a slender-wing airplane would normally not operate in the vortex-breakdown region of angles of attack. Investigation on the effect of vortex breakdown on the buffeting of nearby lifting surfaces, such as tails, was scarce. However, it is known that the vortex from the strake (or leading-edge extension, LEX) may reduce the buffet intensity on the wing before it bursts (p. 109, Ref. 7).

In the present study, the main objective is to predict buffeting on vertical tails induced by LEX vortex bursting. Fundamental equations for structural response will first be derived. Existing theoretical methods for buffet prediction will be reviewed. The present method and some numerical results will then be presented.

2. THEORETICAL DEVELOPMENT

2.1 Formulation of Equations

Structural Equations of Motion:

Let the structural displacement, $Z_a(x, y, t)$, be expressed in terms of normal mode shapes, $\phi_n(x, y)$. Then

$$Z_a(x, y, t) = \sum_{n=1}^{N} q_n(t)\phi_n(x, y) \tag{1}$$

where $q_n(t)$ is the so-called generalized coordinates. It can be shown that the structural equations of motion in forced oscillation in generalized coordinates can be written as (Ref. 13, pp. 131-139, or Ref. 14, Chapter 10):

$$M_n\ddot{q}_n + M_n\omega_n^2 q_n = Q_n \equiv \iint [p_E + p_M]\phi_n(\xi, \eta)d\xi d\eta \tag{2}$$

where

$M_n = \iint \phi_n^2 m dxdy$, the generalized mass

$m(x, y)$ = mass per unit area

ω_n = frequency of the n^{th} normal mode

Q_n = the generalized force.

The generalized force consists of two terms, one being the externally applied force (i.e., the p_E-term) and the other being the force due to structural motion (i.e., the p_M-term).

The p_M-term can be further decomposed in terms of the generalized coordinates as

$$p_M = \sum_{j=1}^{N} \Delta p_j(x, y; \omega, M_\infty)\frac{q_j}{b_o} \tag{3}$$

where Δp_j is the lifting pressure at point (x, y) on the wing caused by the motion of the j^{th} normal mode and b_o is the reference length, e.g. the root semichord. It follows that

$$Q_{Mn} = \sum_{j=1}^{N} \frac{q_i}{b_o} \iint_{S_w} \Delta p_j \phi_n d\xi d\eta = q_\infty \sum_{j=1}^{N} \frac{q_i}{b_o} \iint \Delta C_{p_j} \phi_n d\xi d\eta$$

$$= b_o \ell \frac{q_\infty}{b_o} \sum_{j=1}^{N} A_{nj} q_j \tag{4}$$

where A_{nj} is the generalized aerodynamic force matrix and is defined as

$$A_{nj} = \iint \Delta C_{p_j} \phi_n \, d\bar{\xi} d\bar{\eta} \tag{5}$$

$$\left.\begin{aligned} \xi &= b_o \bar{\xi} \\ \eta &= \ell \bar{\eta} \end{aligned}\right. \tag{6}$$

In Equation (4), q_∞ is the dynamic pressure $(= \rho V_\infty^2/2)$.

Equation (2) can now be written as

$$M_n \ddot{q} + M_n \omega_n^2 q_n - \ell q_\infty \sum_{j=1}^{N} A_{nj} q_j = \iint p_E(\xi, \eta, t) \phi_n(\xi, \eta) d\xi d\eta$$

$$= Q_n^E(t) \tag{7}$$

In the above derivation, neither structural nor viscous dampings have been included. To include the former, ω_n^2 is usually replaced with $\omega_n^2(1 + ig_n)$, where g_n is the structural damping coefficient for the n^{th} mode and is usually taken to be 0.03 if not known experimentally. To account for the latter, $2\zeta M_n \omega_n \dot{q}_n$ is added to the equation with ζ being the damping ratio. Equation (7) becomes

$$M_n\ddot{q}_n + 2\zeta M_n \omega_n \dot{q}_n + M_n \omega_n^2 (1 + ig_n) q_n - \ell q_\infty \sum_{j=1}^{N} A_{nj} q_j = Q_n^E(t) \tag{8}$$

Structural Response to Random Excitation:

If the excitation force $Q_n^E(t)$ is random, it may be represented in a Fourier integral (Chapter 14, Ref. 15),

$$Q_n^E(t) = \int_{-\infty}^{\infty} \bar{Q}_n^E(i\omega) e^{i\omega t} d\omega \tag{9}$$

where

$$\bar{Q}_n^E(i\omega) = \lim_{T\to\infty} \frac{1}{2\pi} \int_{-T}^{T} Q_n^E(t) e^{-i\omega t} dt \tag{10}$$

The displacement $q_n(t)$ will also vary randomly, so that a Fourier integral representation is appropriate.

$$q_n(t) = \int_{-\infty}^{\infty} \bar{q}_n(i\omega) e^{i\omega t} d\omega \tag{11}$$

Substituting Equations (9) and (11) into Equation (8), and requiring the relation to be valid for all t, it is obtained that

$$\bar{q}_n(i\omega)[-M_n\omega^2 + 2i\zeta\omega_n\omega + M_n\omega_n^2(1 + ig_n)] - \ell q_\infty \sum_{j=1}^{n} A_{nj}\bar{q}_j$$
$$= \bar{Q}_n^E(i\omega)$$

or,

$$\sum_{j=1}^{N} \{[-M_n\omega^2 + 2iM_n\zeta\omega_n\omega + M_n\omega_n^2(1 + ig_n)]\delta_{nj} - \ell q_\infty A_{nj}\}\bar{q}_j$$
$$= \bar{Q}_n^E(i\omega) \qquad , \qquad n = 1,\ldots,N \tag{12}$$

Let

$$Z_{nj}(\omega) = [-M_n\omega^2 + 2iM_n\zeta\omega_n\omega + M_n\omega_n^2(1 + ig_n)]\delta_{nj} - \ell q_\infty A_{nj} \tag{13}$$

Note that $Z_{nj}(\omega)$ is called the complex impedance of the system; and its inverse, Z^{-1}, is the so-called structural transfer function.

To describe quantitatively a random response in a meaningful manner, statistical methods must be used. The most important quantity for this purpose is the mean square value. It is defined for a random function F(t) as (Ref. 15)

$$\overline{F^2(t)} = \lim_{T\to\infty} \frac{1}{2T} \int_{-T}^{T} F^2(t)dt = \lim_{T\to\infty} \frac{1}{2T} \int_{-T}^{T} F(t) \int_{-\infty}^{\infty} f(i\omega)e^{i\omega t}d\omega dt$$

$$= \lim_{T\to\infty} \frac{1}{2T} \int_{-\infty}^{\infty} f(i\omega) \int_{-T}^{T} F(t)e^{i\omega t}dtd\omega$$

$$= \lim_{T\to\infty} \frac{1}{2T} \int_{-\infty}^{\infty} f(i\omega)2\pi f^*(i\omega)d\omega = \int_{-\infty}^{\infty} \lim_{T\to\infty} \frac{\pi|f(i\omega)|^2}{T} d\omega \tag{14}$$

where f^* is the complex conjugate of f. Define

$$S(\omega) = \lim_{T\to\infty} \frac{\pi f(i\omega)f^*(i\omega)}{T} \tag{15}$$

Equation (14) becomes

$$\overline{F^2(t)} = \int_{-\infty}^{\infty} S(\omega)d\omega \tag{16}$$

In case the random function depends also on space coordinates, the definition of $S(\omega)$ must be modified. For the generalized force of the n^{th} mode, $Q_n^E(t)$, it is defined as (Equation 7)

$$Q_n^E(t) = \int p_E(r, t)\phi_n(r)dA \tag{17}$$

where space coordinates (ξ, η) are now represented by r. The Fourier spectrum of Q_n^E is

$$\bar{Q}_n^E(i\omega) = \iint \bar{p}_E(i\omega)\phi_n(r)dA \tag{18}$$

The power spectrum of the n^{th} generalized force is given by

$$S_n(\omega) = \lim_{T\to\infty} \frac{\pi}{T} \bar{Q}_n^E(i\omega)\bar{Q}_n^{*E}(i\omega)$$

$$= \lim_{T\to\infty} \frac{\pi}{T} \int_A \bar{p}_E(i\omega)\phi_n(r_1)dA_1 \int_A \bar{p}^*(i\omega)\phi_n(r_2)dA_2$$

$$= \lim_{T\to\infty} \frac{\pi}{T} \iint_{AA} \phi_n(r_1)\phi_n(r_2) \frac{1}{4\pi^2} \int_{-T}^{T} \int_{-T}^{T} p_E(r_1, t_1)p_E(r_2, t_2)$$

$$\cdot\, e^{i\omega(t_1-t_2)} dt_1 dt_2 dA_1 dA_2 \tag{19}$$

Let $t_2 - t_1 = \tau$. Equation (19) can be written as

$$S_n(\omega) = \iint_{AA} \phi_n(r_1)\phi_n(r_2) \lim_{T\to\infty} \frac{1}{T} \frac{1}{4\pi} \int_{-T}^{T} \int_{-T}^{T} p_E(r_1, t_1)p_E(r_2, t + \tau)$$

$$\cdot\, e^{-i\omega\tau} dt_1 d\tau dA_1 dA_2$$

$$= \iint_{AA} \phi_n(t_1)\phi_n(r_2) \int_{-\infty}^{\infty} \frac{1}{2\pi} R_{12}(r_1, r_2, \tau)e^{-i\omega\tau} d\tau dA_1 dA_2 \tag{20}$$

where

$$R_{12}(r_1, r_1\ \tau) = \lim_{T\to\infty} \frac{1}{2T} \int_{-T}^{T} p_E(r_1, t_1)p_E(r_2, t_1 + \tau)dt_1 \tag{21}$$

is known as the space-time correlation or cross correlation function. Define

$$S_{12}(r_1, r_2, \omega) = \frac{1}{2\pi}\int_{-\infty}^{\infty} R_{12}(r_1, r_2, \tau)e^{-i\omega\tau}d\tau \tag{22}$$

the cross power spectral density of pressures at r_1 and r_2. It follows that

$$S_n(\omega) = \int_A \phi_n(r_1) \int_A \phi_n(r_2)S_{12}(r_1, r_2\ \omega)dA_2dA_1 \tag{23}$$

$S(\omega)$ or $S_n(\omega)$ is known as the power spectral density. This is because if $F(t)$ were a current, the power developed by this current as it passed through a resistance of one ohm would be $F^2(t)$.

Returning to calculation of the total response, Equations (11) - (13) show that the amplitude of the motion in the n^{th} mode is

$$q_n(t) = \int_{-\infty}^{\infty} \left([Z(\omega)]^{-1}\{\bar{Q}^E(i\omega)\}\right)_n e^{i\omega t}d\omega \tag{24}$$

The total displacement is therefore

$$Z_a(x, y, t) = \sum_{n=1}^{N} \int_{-\infty}^{\infty} \left([Z(\omega)]^{-1}\{\bar{Q}^E(i\omega)\}\right)_n \phi_n(x, y)e^{i\omega t}d\omega \tag{25}$$

from which the Fourier spectrum of the total displacement can be identified as

$$\sum_{n=1}^{N} \left([Z(\omega)]^{-1}\{\bar{Q}^E(i\omega)\}\right)_n \phi_n(x, y) \tag{26}$$

and the corresponding power spectrum is

$$S_w(\omega) = \lim_{T\to\infty} \frac{\pi}{T} \left\{ \sum_{n=1}^{N} \left([Z(\omega)]^{-1}\{\bar{Q}^E(i\omega)\}\right)_n \phi_n(x, y) \right\}\left\{ \sum_{n=1}^{N} \left([Z(\omega)]^{-1} \{\bar{Q}^E(i\omega)\}\right)_n^* \phi_n(x, y)\right\} \tag{27}$$

Once $S_w(\omega)$ is known, the mean square value of displacement can be obtained as

$$\overline{Z_a^{\,2}} = \int_{-\infty}^{\infty} S_w(\omega)d\omega \tag{28}$$

Responses in accelerations, loads, moments, and stresses, etc., can be similarly formulated.

Equation (27) is difficult to simplify because of mode coupling through the generalized aerodynamic force matrix, A_{nj}. If the aerodynamic force due to structural motion is ignored, or $A_{nj} \approx 0$ if $n \neq j$, then Equation (27) can be further simplified. Let

$$Z_{nn}(\omega) = M_n[-\omega^2 + 2i\zeta\omega_n\omega + \omega_n^{\,2}(1 + ig_n)] - \ell q_\infty A_{nn} \tag{29}$$

Equation (27) can be rewritten as

$$S_w(\omega) = \lim_{T\to\infty} \frac{\pi}{T} \left\{ \sum_{n=1}^{N} \frac{\bar{Q}_n^{\,E}(i\omega)\phi_n(x,\ y)}{Z_{nn}(\omega)} \right\}\left\{ \sum_{n=1}^{N} \frac{\bar{Q}_n^{*E}\ (i\omega)\phi_n(x,\ y)}{Z_{nn}^{\ *}(\omega)} \right\} \tag{30}$$

After multiplying this out, it can be obtained that

$$\begin{aligned} S_w(\omega) &= \lim_{T\to\infty} \frac{\pi}{T} \left\{ \sum_{n=1}^{N} \frac{\bar{Q}_n^{\,E}\ \bar{Q}_n^{E*}\ \phi_n^{\,2}(x,\ y)}{Z_{nn}Z_{nn}^{\ *}} + \right. \\ &\quad \left. + \sum_{\substack{j=1 \\ j\neq\ell}}^{N} \sum_{\ell=1}^{N} \frac{\bar{Q}_j^{\,E}\bar{Q}_\ell^{\,*E}}{Z_{jj}Z_{\ell\ell}^{\ *}}\ \phi_j\phi_\ell \right\} \\ &= \sum_{n=1}^{N} \frac{\phi_n^{\,2}(x,\ y)}{|Z_{nn}(\omega)|^2} \int_A \phi_n(r_1) \int_A \phi_n(r_2)S_{12}(r_1,\ r_2,\ \omega)dA_2dA_1 + \\ &\quad + \sum_{\substack{j=1 \\ j\neq\ell}}^{N} \sum_{\ell=1}^{N} \frac{\phi_j(x,y)\phi_\ell(x,\ y)}{Z_{jj}(\omega)Z_{\ell\ell}^{\ *}(\omega)} \int_A \phi_j(r_1) \int_A \phi_\ell(r_2)S_{12}(r_1,\ r_2,\ \omega)dA_2dA_1 \end{aligned} \tag{31}$$

The first series of Equation (31) represents the sum of the spectra of the responses in individual modes. The second series represents the correlation between the responses in different modes. The second series can be ignored if only two or three modes are present and their natural frequencies are widely separated (Ref. 15).

In Reference 16, the cross power spectral density was specified in exponential functions with coefficients determined by experiment.

2.2 Existing Theoretical Methods for Buffet Prediction

All existing theoretical methods require some types of experimental data to work with. Sophistication of these required data distinguishes one method from the other.

Cunningham and Benepe (Refs. 17 and 18):

Pressure power spectral densities are first converted into pressure distributions over the wing for each frequency. The doublet lattice method (DLM) is then used to calculate induced pressures on the tail due to downwash produced by the wing buffet pressures. The wing and tail pressures are used in the DLM to calculate the generalized aerodynamic forces. The whole equation (12) is used without simplification. The calculation is similar to that for gust response.

B. H. K. Lee (Ref. 19):

Again, Equation (12) is used. However, the cross correlation function S_{12} in Equation (23) is either taken to be constant over an aerodynamic panel or asumed to vary exponentially in space.

Mullans and Lemley (Ref. 20):

The fluctuating pressure on a rigid model is again used to calculate the generalized aerodynamic forces. However, the aerodynamic forces due to wing vibration, i.e. A_{nj}-terms, are ignored.

J. G. Jones (Refs. 21 and 22):

It is assumed that each mode behaves as a single-degree-of-freedom system:

$$M_n \ddot{q}_n + 2M_n \zeta\omega_n \dot{q}_n + M_n \omega_n^2 q_n = Q_n^E(t) \tag{32}$$

The aerodynamic forces due to wing motion are ignored. Applying the Fourier transform to Equation (32), it is obtained that

$$M_n(-\omega^2 + 2i\zeta\omega_n\omega + \omega_n^2)\bar{q}_n = \bar{Q}_n^E(i\omega) \tag{33}$$

Using the definition of power spectral density, Equation (15), the power spectral density of the response can be obtained:

$$S_q(\omega) = \frac{S_{\bar{Q}_n}(\omega)}{M_n^2(-\omega^2 + 2i\zeta\omega_n\omega + \omega_n^2)(-\omega^2 - 2i\zeta\omega_n\omega + \omega_n^2)} \tag{34}$$

The mean square value of q_n is therefore

$$\overline{q_n^2(t)} = \int_{-\infty}^{\infty} S_q(\omega)d\omega$$

$$= \int_{-\infty}^{\infty} \frac{S_{\bar{Q}_n}(\omega)}{M_n^2 H_n(\omega) H_n^*(\omega)} d\omega \tag{35}$$

where

$$H_n(\omega) = -\omega^2 + 2i\zeta\omega_n\omega + \omega_n^2 \tag{36}$$

The main contribution to the value of the integral in Equation (35) comes from the peak response at $\omega = \omega_n$. If $S_{\bar{Q}}(\omega)$ is assumed not to vary appreciably in the neighborhood of ω_n, it can be factored out of the integral in Equation (35) and the result integrated analytically based on the residue theorem in the theory of a complex variable. Results are available in Reference 23 (p. 218). Therefore, Equation (35) can be reduced to

$$\overline{q_n{}^2(t)} \approx \frac{\pi}{2} \frac{S_{\bar{Q}_n}(\omega_n)}{M_n{}^2 \zeta \omega_n{}^3} \tag{37}$$

Instead of $\overline{q_n{}^2(t)}$, Jones determined $\overline{\ddot{q}_n{}^2}$, the mean square acceleration. Note that the Fourier transform of $\ddot{q}_n$ is

$$\bar{\ddot{q}}_n = (i\omega)^2 \bar{q}_n \tag{38}$$

Therefore,

$$S_{\ddot{q}} = \frac{(i\omega)^4 S_{\bar{Q}_n}(\omega)}{M_n{}^2 H_n(\omega) H_n{}^*(\omega)} \tag{39}$$

The result for $\overline{\ddot{q}_n{}^2}$ is (Ref. 21)

$$\overline{\ddot{q}_n{}^2} \approx \frac{1}{8} \frac{\omega_n}{M_n{}^2 \zeta} S_{\bar{Q}_n}(\omega_n) \tag{40}$$

Let

$$S_{\bar{Q}_n}(\omega) = \frac{E^2 \bar{c}}{V} (q_\infty S)^2 \tag{41}$$

where q_∞ is the freestream dynamic pressure and E^2 is a nondimensional aerodynamic excitation parameter. It follows that

$$E = 2\sqrt{2}\ \left(\frac{V}{\bar{c}\omega_n}\right)^{1/2}\left(\frac{M_n}{S}\right)\left(\frac{\zeta^{1/2}\bar{\bar{q}}_n^{\,2}}{q_\infty}\right) \tag{42}$$

$$\bar{\bar{q}}_n = \frac{1}{2\sqrt{2}}\ \left(\frac{\bar{c}\omega_n}{V\zeta}\right)^{1/2} E\ \frac{q_\infty S}{m} \tag{43}$$

To use Equation (43), the damping ratio (ζ) is needed. It consists of both the structural damping (ζ_s) and the aerodynamic damping (ζ_a). The latter arises from the effective angle of attack due to wing vibration and is given by

$$2M_n \zeta_a \omega_n \dot{q}_n = 2q_\infty SK\ \frac{\dot{q}_n}{V} \tag{44}$$

where K, the aerodynamic damping parameter, is a nondimensional parameter depending on the mode shape, the wing planform, and the sectional lift-curve slope. Equation (44) is assumed applicable to both attached and separated flows. It follows from Equation (44) that

$$\zeta_a = \frac{q_\infty SK}{M_n \omega_n V} \tag{45}$$

$$K = \frac{M_n \omega_n V \zeta_a}{q_\infty S} \tag{46}$$

In Jones' method, both E and K are assumed to be independent of the scale effect. In other words, their values determined from model test can be applied to full-scale airplanes. Practical procedures of applying this method were discussed by Butler and Spavins in Reference 24. They are as follows:

(a) Determine modal frequency ω_n, the mode shape, generalized mass M_n, and structural damping ζ_s from wind-off resonance tests on model and aircraft. Note that the relevant model mode shape must be approximately correct.

(b) Measure rms acceleration or bending moment $\overline{C_B}$ at a point on the wing, the total damping ζ, flow velocity V, and dynamic pressure q_∞, at a given Mach number and angle of attack in wind-tunnel tests.

(c) Relate $\overline{C_B}$ to q_n in generalized coordinates using the mode shape (see Section 2.3).

(d) Calculate E from Equation (42).

(e) Calculate K from Equation (46).

(f) Calculate total damping of aircraft by adding calculated ζ_a from Equation (45) to the measured ζ_s.

(g) Predict rms acceleration or bending moment at a point on the aircraft wing from Equation (43) using the measured aircraft mode shape.

<u>Mabey's Method</u> (Refs. 25 and 26):

This method was developed to determine qualitatively the flight conditions for light, moderate and heavy buffeting for the full-scale aircraft from measurement of wing root bending moment of a conventional wind-tunnel model. It is assumed that the wing responds to buffeting pressures in somewhat the same way as to the wind-tunnel turbulence at the wing fundamental frequency.

Let the tunnel unsteadiness $\sqrt{nF(n)}$ be defined so that the total rms pressure fluctuation coefficient is given by

$$\frac{\overline{p^2}}{q_\infty^2} = \int_{-\infty}^{\infty} [nF(n)] \frac{1}{n} dn \qquad (47)$$

where

$n = f_o w/V$

w = tunnel width

f = wing fundamental bending frequency in cycles per second

V = freestream velocity.

Define

$$C_{BB}(M, \alpha) = \text{wing-root strain signal}/q_\infty \qquad (48)$$

Before the onset of flow separation on the model, $C_{BB}(M, \alpha)$ has been shown experimentally to be constant equal to $C_{BB}(M, \alpha = 0)$. This is the portion of the model response caused by the tunnel unsteadiness $\sqrt{nF(n)}$

. Assume that

$$C_{BB}(M, \alpha = 0°) = K_B\sqrt{nF(n)} \qquad (49)$$

where K_B is a scaling factor. Then

$$C_{BB}'(M, \alpha = 0°) = \frac{1}{K_B} C_{BB}(M, \alpha = 0°) = \sqrt{nF(n)} \qquad (50)$$

Beyond buffet onset, $C_{BB}(M,\alpha)$ is increased due to wing buffet pressures. Let

$$C_{BB}''(M, \alpha) = [C_{BB}'(M, \alpha)^2 - C_{BB}'(M, \alpha = 0°)^2]^{1/2} \qquad (51)$$

The angle of attack at which $C_{BB}''(M, \alpha)$ first differs from zero is the buffet-onset angle. From correlations on nine models of fighter aircraft, the following buffeting criteria were suggested:

Buffet onset	$C_{BB}'' = 0$
Light buffeting	$C_{BB}'' = 0.004$
Moderate buffeting	$C_{BB}'' = 0.008$
Heavy buffeting	$C_{BB}'' = 0.016$

Note that in using this method, the total damping of the wing fundamental mode should be relatively constant, independent of wind velocity and density. This is true if models with solid wings of steel or light alloy are used, because in this case the structural damping will predominate. No mass, stiffness (or ω_o) and damping for both models and aicraft are needed. It is useful during comparative tests for projects with alternative wing designs.

Thomas' Method (Ref. 27):

At transonic speeds, buffeting is closely connected with flow separation due to shock-boundary layer interaction and shock oscillations. Using conventional boundary layer methods, the development of boundary layer on airfoils at transonic speeds can be calculated. By comparing calculations with experimental results, Thomas postulated that buffet onset started if the point of rear separation coming from the trailing edge reached 90% of the airfoil chord.

Redeker (Ref. 28) extended this method to infinite yawed wings by using the pressure distribution on a section normal to the leading edge and applying a three-dimensional compressible boundary layer method.

Further extension of Thomas' method to finite wings was made by Proksch (Ref. 28). A buffeting coefficient (C_{Bi}) is defined which is directly related to the rms value of the wing root bending moment. It is assumed that the fluctuations of the wing root bending moment are proportional to the integral evaluated along the wing span of the product of local lift fluctuations and the distance from the wing root ($\eta - \eta_R$). A further assumption is that the local lift oscillations caused by flow separation are proportional to length $\ell_s(\eta)$ of the separated flow at a spanwise station of the wing. It follows that

$$C_{Bi} = \int_{\eta_R}^{1} \frac{\ell_s(\eta)}{\bar{c}} (\eta - \eta_R) d\eta \sim \sqrt{\overline{C_B^2}} \tag{52}$$

2.3 The Present Proposed Method

Theoretically, it is possible to use Equations (23) - (28) to calculate buffet response in the most general way. However, it would be an expensive undertaking because extensive fluctuating pressure measurement on empennage must be made. In addition, these fluctuating pressures are configuration dependent and vary with flight conditions. Therefore, a method similar to Jones' in concept is proposed.

In developing the proposed method, the following steps are needed.

(a) Buffeting vortex strength in the burst region must be known. It is known that steady vortex strength from a slender wing or LEX can be estimated by the method of suction analogy (Ref. 29). Similarly, buffeting vortex strength can also be estimated if buffeting normal force data on slender wings are available. This is because any buffeting on slender wings can be assumed to be caused by the leading edge vortex. A limited amount of such data was published in References 4 and 9.

Let c_s be the sectional suction coefficient. Based on the suction analogy, the vortex lift is proportional to c_s. The vortex lift can also be expressed in terms of the vortex strength Γ through Kutta-Joukowski theorem as

$$\frac{1}{2}\rho V_\infty^{\ 2} c_s c dy = \rho \Gamma w_{\ell e} d\ell \tag{53}$$

where $w_{\ell e}$ is the normal velocity at the leading edge and $d\ell$ is the vortex length along the leading edge. It follows that

$$\frac{\Gamma}{V_\infty} d\ell = \frac{1}{2} \frac{c_s c}{w_{\ell e}/V_\infty} dy$$

and

$$\Gamma_t = \int \frac{\Gamma}{V_\infty} d\ell = \frac{1}{2} \int_o^{b/2} \frac{c_s c}{w_{\ell e}/V_\infty} dy$$

The average strength per unit length is

$$\bar{\Gamma}_t = \Gamma_t / S_{\ell e} = \frac{1}{2S_{\ell e}} \int_o^{b/2} \frac{c_s c}{w_{\ell e}/V_\infty} dy \tag{54}$$

where $S_{\ell e}$ is the length of the leading edge. The unsteady aerodynamics program of Reference 30 was revised to calculate $\bar{\Gamma}_t$. In the calculation, the buffeting normal force is obtained by assuming a vertical oscillation of constant amplitude over the region of predicted vortex breakdown. The latter was calculated by a semi-empirical method to interpolate or extrapolate experimental data (Ref. 31). The amplitude was adjusted to match the experimental data on fluctuating normal force coefficients in Reference 9. Unfortunately, only data at a low frequency for some delta wings were measured in Reference 9. On the other hand, the power spectrum over a range of frequencies at the vortex-breakdown angle of attack for the BAC 221 configuration is available (Fig. 24 of Ref. 4). Unless additional data are available in the future, for the present purpose the low-frequency data of Reference 9 will be used to derive the buffeting strength for a range of angles of attack. At other frequencies, the strength will be multiplied by a ratio obtained from data for the BAC 221 in Reference 4.

(b) The root bending moment can be calculated as

$$M_o(t) = \int_o^{b/2} [\ell_E(y, t) + \ell_M(y, t) - \left(\sum_{n=1}^{N} \ddot{q}_n(t)\phi_n(y)\right)m(y)]ydy \tag{55}$$

where ℓ_E is the sectional lift due to external forces, ℓ_M is the sectional lift due to structural motion and the last term is the inertial forces. For a rigid wing, the last two terms can be ignored. In Jones' analysis, ℓ_M was also ignored. Using the notation of Equation (4), ℓ_M can be written as

$$\ell_M(y,\ t) = q_\infty \sum_{n=1}^{N} \sum_{j=1}^{N} \frac{q_j}{b_o} \int \Delta C_{p_j}(x,\ y)(\phi_n(x,\ y) m dx \tag{56}$$

Let the Fourier transform of $\ell_E(y,\ t)$ be written as

$$\overline{\ell_E}\,(y,\ t) = \sum_{n=1}^{N} \bar{\ell}_{E_n}(y,\ i\omega)\bar{Q}_n^{\ E}(i\omega) \tag{57}$$

where $\bar{\ell}_{E_n}$ is the sectional lift due to a unit generalized force in the n^{th} mode. Applying the Fourier transform to Equation (55), it is obtained that

$$\bar{M}_o(i\omega) = \int_o^{b/2} [\sum_{n=1}^{N} \bar{\ell}_{E_n}(y,\ i\omega) + \frac{\bar{\ell}_M}{\bar{Q}_n^{\ E}} + \sum_{n=1}^{N} \frac{\omega^2}{M_n H(\omega)}\, m\phi_n(y)]\bar{Q}_n^{\ E} y dy$$

$$= \sum_{n=1}^{N} [BM_{E_n}(i\omega) + BM_{M_n}(i\omega) + \frac{\omega^2}{M_n H_n(\omega)} \int m\phi_n(y) y\ dy]\bar{Q}_n^{\ E}$$

$$= H_{BM}(\omega)\bar{Q}_n^{\ E}(i\omega) \tag{58}$$

where Equation (33) has been used. $H_{BM}(\omega)$ is the bending moment transfer function and is defined as

$$H_{BM}(\omega) = \sum_{n=1}^{N} [BM_{E_n}(i\omega) + BM_{M_n}(i\omega) + \frac{\omega^2}{M_n H_n(\omega)} \int_o^{b/2} m\phi_n(y) y\ dy] \tag{59}$$

The power spectral density of $M_o(t)$ is therefore

$$S_{BM}(\omega) = |H_{BM}(\omega)|^2 S_{\bar{Q}_n}(\omega) \tag{60}$$

where $S_{\bar{Q}_n}$ is the power spectral density of the buffeting excitation. For a rigid wing, Equation (60) can be simplified to

$$S_{BM}(\omega) = |BM_E(i\omega)|^2 S_{\bar{Q}_n}(\omega) \tag{61}$$

In applications, BM_E will be calculated by assuming a unit buffeting excitation over the region of vortex breakdown at a range of frequencies. The mean square value of bending moment is then given by

$$\overline{M_o^2} = \int_{-\infty}^{\infty} S_{BM}(\omega)d\omega = 2\int_{o}^{\infty} S_{BM}(\omega)d\omega \tag{62}$$

which is to be integrated numerically.

(c) Since only total force power spectrum, instead of pressure power spectrum, will be used, it is assumed that the pressure fluctuations at every point on the wing are perfectly correlated in space and are in phase. Based on this assumption, Mabey and Butler showed that the total force power spectral density was proportional to the pressure power spectral density (Ref. 11). The results from this were shown to be reasonably accurate.

In the present application to empennge buffeting due to a LEX vortex, those unsteady buffeting vortices, once generated, will be convected downstream in accordance with the general principle of unsteady aerodynamics.

(d) With the power spectral density of buffeting vortex strength determined at a given flight condition, fluctuating normal velocity will be induced on the empennage. By satisfying the usual flow tangency condition, buffeting pressure spectral density on the empennage can be calculated. From the buffeting pressure spectral density, the power spectrum of bending moment or other aerodynamic characteristics can be determined. The root mean square values of root bending moment are calculated by using Equation (62).

(e) Similar to Jones' method, the calculation of buffet response requires structural data, such as mode shapes, generalized mass, and damping ratio.

(f) In applications to empennage buffeting, the locations of LEX vortex bursting will be based on experimental data.

3. SOME NUMERICAL RESULTS AND DISCUSSIONS

In Reference 9, data for a cambered and a flat model of 70-degree delta wing are available at a frequency parameter n of 0.05, where

$$n = f\bar{c}/V_\infty \tag{63}$$

and f is the frequency in cycles per second. This is converted into the conventional reduced frequency k by multiplying by 2π. Before vortex breakdown, the normal force fluctuation is assumed to be caused by tunnel flow unsteadiness. The resulting amplitudes of vertical oscillation (or buffeting excitation) in the vortex-breakdown region needed to produce the experimental mean square values of normal force coefficients are shown in Figure 1. At each angle of attack, a buffeting vortex strength $\bar{\Gamma}_t$ can be calculated from Equation (54). The same expression is used to calculate the vortex strength $\bar{\Gamma}_s$ in steady flow using the steady-flow c_s. Now, if Figure 1 is replotted in terms of the ratio of buffeting to steady vortex strengths, $R_{b/s}$:

$$R_{b/s} = \bar{\Gamma}_t/\bar{\Gamma}_s \tag{55}$$

those two curves in Figure 1 tend to collapse into one as shown in Figure 2. From Figure 2, it can be concluded that the buffeting vortex strength is a function of steady-flow vortex strength and $\Delta\alpha$, where $\Delta\alpha$ is the incremental angle beyond that of vortex breakdown which occurs at the trailing edge.

The method is now used to analyze a cambered delta wing of 65-degree sweep as shown in Figure 3. To find the buffeting characteristics for a flat 65-degree delta wing, it is assumed that the buffeting excitation (AMPLG) for the latter is equal to that for a cambered 65-degree delta wing if $R_{b/s}$ is the same. Therefore, at a given $\Delta\alpha$, $R_{b/s}$ is obtained from Figure 3. Using this $R_{b/s}$, AMPLG can be determined from Figure 4. Note that Figure 4 was constructed from the experimental data for a cambered wing. The resulting buffeting excitation amplitudes for a flat delta wing are plotted in Figure 5. This type of data extrapolation must be used with caution. This is done here mainly because test data for fluctuating normal force coefficients of the flat 65-degree delta wing are not available. However, test data for the rms values of root bending moment are available for comparison with predicted results.

The buffeting force characteristics for both 70-degree and 65-degree delta wings are compared in Figure 6. The difference between these two curves arises mainly from differences in forward progression rate of breakdown points.

To check the theory, test data of Reference 32 for the root bending moment will be used. Static bending moment coefficients based on $\bar{c}$ are presented in Figure 7. Calculated results from Reference 29 are also presented for comparison. It is seen that at high angles of attack, the theory overpredicts the root bending moment. This is because the theory does not account for the inboard movement of vortex flow as the angle of attack is increased. An investigation to correct this discrepancy is under way.

To calculate the dynamic response of a rigid wing, Equations (61) and (62) will be used. To calculate the transfer function (BM_E) for the root bending moment, a unit amplitude of vertical excitation is prescribed over the region of vortex breakdown at each frequency. Some results are presented in Figure 8. The corresponding power spectral densities for the excitation are obtained by multiplying the values in Figure 5 (for a low frequency only) by a ratio obtained from Figure 24 of Reference 4 for other frequencies. The results are shown in Figure 9. Equation (62) is then integrated by the trapezoidal rule to produce the mean square values of root bending moment. The rms values are presented in Figure 10. Note that experimental data were obtained at resonant frequencies of the fundamental bending mode. Since the spectral density is higher at higher frequencies (Fig. 9), the calculated response of a rigid wing tends to be similar to the test data at a high frequency, although the magnitudes are underpredicted. It is expected that the prediction can be improved if the structural flexibility is accounted for.

4. WORK UNDER WAY

All geometric data for the F-18 have now been acquired and computerized in the input format for the VORSTAB code (Ref. 29). Wing sectional aerodynamic characteristics are being calculated with the Eppler's code (Ref. 33) to form a part of the input. At a given angle of attack, the wake and the LEX vortices will be allowed to deform until an equilibrium position is reached. The resulting position of the LEX vortices relative to the vertical fins of F-18 will then be input to the unsteady aerodynamics program of Reference 30 to calculate the fin buffeting. For this purpose, the program of Reference 30 must be modified to include the effect of large geometric dihedral angles. Again, only the response of rigid fins will be calculated in the current plan.

REFERENCES

1. Triplett, W. E., "Pressure Measurements on Twin Vertical Tails in Buffeing Flow," Journal of Aircraft, Vol. 20, November 1983, pp. 920-925.

2. Lemley, C. E., and Mullans, R. E., "Buffeting Pressures on a Swept Wing in Transonic Flight--Comparison of Model and Full Scale Measurements," AIAA Paper 73-311.

3. Hwang, C., and Pi, W. S., "Transonic Buffet Behavior of Northropp F-54 Aircraft," AGARD R-624, 1974.

4. Mabey, D. G., "A Review of Some Recent Research on Time-Dependent Aerodynamics," Aeronautical Journal, February 1984, pp. 23-37.

5. Mabey, D. G., "Beyond the Buffet Boundary," Aeronautical Journal, April 1973, pp. 201-214.

6. John, H., "Critical Review of Methods to Predict the Buffet Capability of Aircraft," AGARD R-623, 1974.

7. AGARD AR-82, "The Effects of Buffeting and Other Transonic Phenomena on Maneuvering Combat Aircraft," 1975.

8. Mabey, D. G., "Measurements of Buffeting on Slender Wing Models," British ARC CP-917, March 1966.

9. Earnshaw, P. B., and Lawford, J. A., "Low-Speed Wind-Tunnel Experiments on a Series of Sharp-Edged Delta Wings," British ARC R&M 3424, 1966.

10. Lovell, D. A., and Owen, T. B., "Low-Speed Wind-Tunnel Measurements of Surface Pressure Fluctuations on Two Slender-

Wing Models," British ARC C.P. 1154, Sept. 1970.

11. Mabey, D. G., and Butler, G. F., "Measurements of Buffeting on Two 65° Delta Wings of Different Materials," AGARD CP-226, 1977.

12. Rose, R., and Nicholas, O. P., Flight and Tunnel Measurements of Pressure Fluctuations on the Upper Surface of the Wing of a Venom Aircraft with a Sharpened Leading-Edge," British CP 1032, November 1967.

13. Dowell, E. H., Curtiss, H. C., Jr., Scanlan, R. H., and Sisto, F., "A Modern Course in Aeroelasticity," Sijthoff & Noordhoff, 1980.

14. Bisplinghoff, R. L., Ashley, H., and Halfman, R. L., "Aeroelasticity," Addison-Wesley, 1955.

15. Richards, E. J., and Mead, D. J., "Noise and Acoustic Fatigue in Aeronautics ," John Wiley & Sons, 1968.

16. Houbolt, J. C., "Mathematical Modeling and Response Evaluation for the Fluctuating Pressures of Aircraft Buffeting," AGARD-R-630, 1975.

17. Cunningham, A. M., Jr., and Benepe, D. B., Sr., "Prediction of Transonic Aircraft Buffet Response," Paper No. 3 in AGARD-CP-226, Unsteady Airloads in Separated and Transonic Flow, 1977.

18. Cunningham, A. M., Jr., Benepe, D. B., Watts, D., and Waner, P. G., "A Method for Predicting Full Scale Buffet Response with Rigid Wind Tunnel Model Fluctuating Pressure Data. Volume I: Prediction Method, Development and Assessment," NASA CR 3035, November 1978.

19. Lee, B. H. K., "A Method for Predicting Wing Response to Buffet Loads," Journal of Aircraft, Vol. 21, January 1984, pp. 85-87.

20. Mullans, R. E., and Lemley, C. E., "Buffet Dynamic Loads During Transonic Maneuvers," AFFDL TR-72-46, September 1972.

21. Jones, J. G., "Modelling of Systems with a High Level of Internal Fluctuations," AGARD-CP-172, 1974.

22. Butler, G. F., and Jones, J. G., "The Prediction of Buffeting Response in Flight from Wind-Tunnel Measurements on Models of Conventional Construction," Aeronautical Journal, August/September 1984, pp. 317-325.

23. Gradshteyn, I. S., and Ryzhik, I. M., "Table of Integrals, Series, and Products," Academic Press, 1965.

24. Butler, G. F., and Spavins, G. R., "Preliminary Evaluation of a Technique for Predicting Buffet Loads in Flight from Wind-Tunnel Measurements on Models of Conventional Construction," Paper No. 23, AGARD CP-204, Prediction of Aerodynamic Loading, 1977.

25. Mabey, D. G., "An Hypothesis for the Prediction of Flight Penetration of Wing Buffeting from Dynamic Tests on Wind Tunnel Models," British ARC CP 1171, October 1970.

26. Mabey, D. G., "Prediction of the Severity of Buffeting," Paper No. 7, AGARD-LS-94, Three Dimensional and Unsteady Separation at High Reynolds Numbers, 1978.

27. Thomas, F., and Redeker, G., "A Method for Calculating the Transonic Buffet Boundary Including the Influence of Reynolds Number," AGARD CP-83, 1971.

28. Redeker, G., and Proksch, H. J., "The Prediction of Buffet Onset and Light Buffet by Means of Computational Methods," Paper No. 22, AGARD CP-204, Prediction of Aerodynamic Loading, 1977.

29. Lan, C. E., "VORSTAB--A Computer Program for Calculating Lateral-Directional Stability Derivatives with Vortex Flow Effect," NASA CR-172501, January 1985.

30. Lan, C. E., "The Unsteady Suction Analogy and Applications," AIAA Journal, Vol. 20, December 1982, pp. 1647-1656.

31. Lan, C. E., and Hsu, C. H., "Effects of Vortex Breakdown on Longitudinal and Lateral-Directional Aerodynamics of Slender Wings by the Suction Analogy," AIAA Paper 82-1385, 1982.

32. Boyden, R. P., Jr., and Johnson, W. G., Jr., "Results of Buffet Tests in a Cryogenic Wind Tunnel," NASA TM 84520, 1982.

33. Eppler, R., and Somers, D. M., "A Computer Program for the Design and Analysis of Low-Speed Airfoils," NASA TM-80210, 1980.

ORIGINAL PAGE IS
OF POOR QUALITY

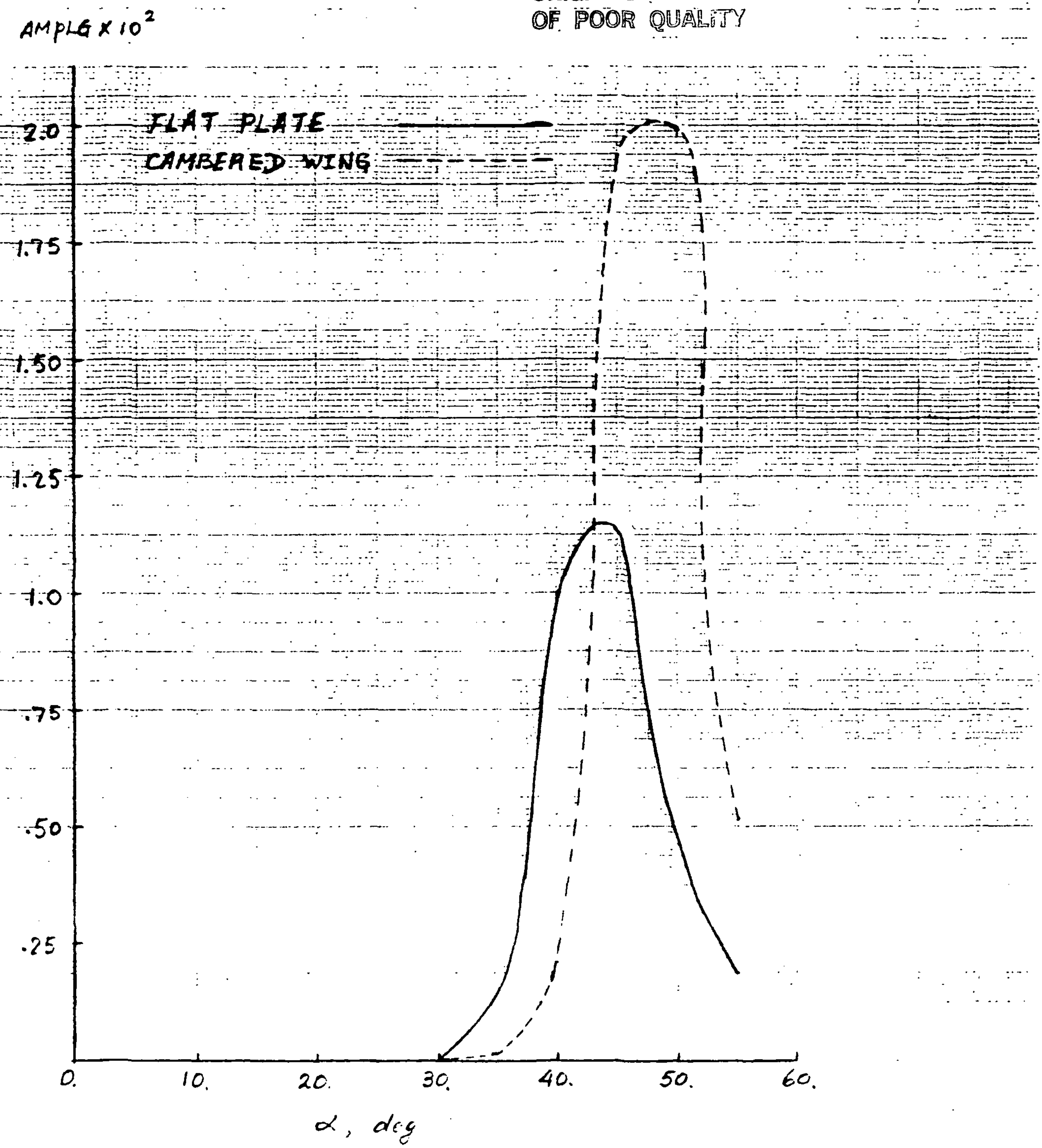

FIG 1. PLUNGING AMPLITUDE REQUIRED VS. α FOR Λ_{LE} = 70 deg DELTA WING. η = 0.05.

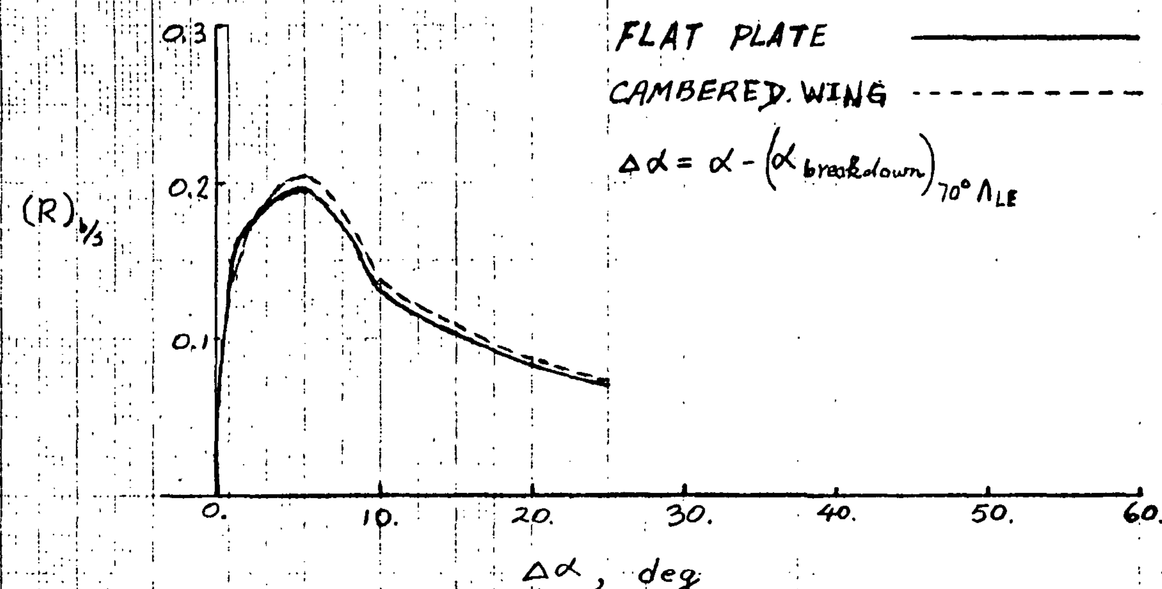

FIG 2. Buffeting Vortex Strength / Steady Vortex Strength VS. $\Delta\alpha$ For $\Lambda_{LE} = 70^\circ$ Delta Wing. $n = 0.05$.

ORIGINAL PAGE IS
OF POOR QUALITY

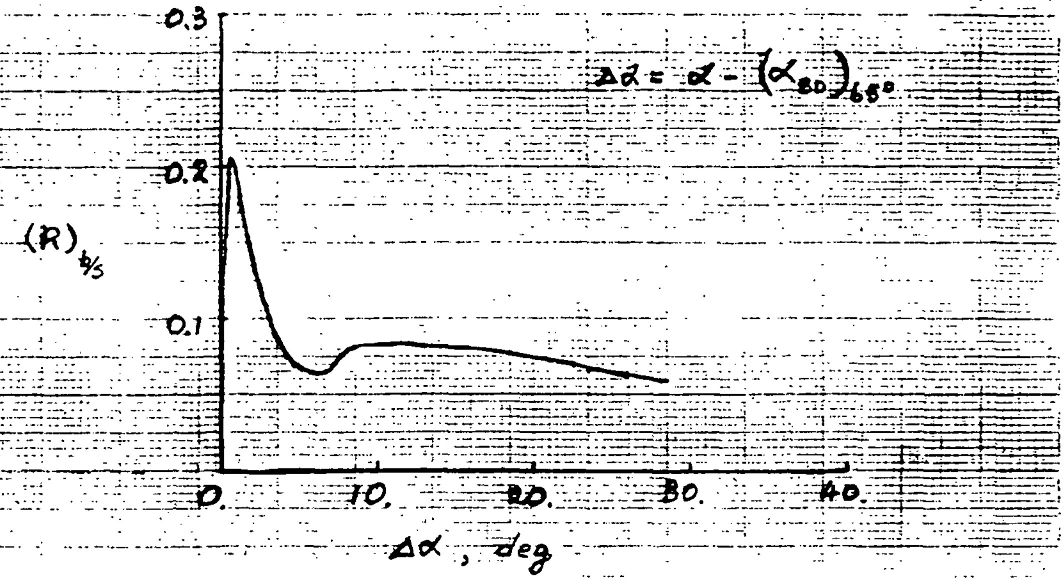

FIG 3. Buffeting Vortex Strength / Steady Vortex Strength VS. $\Delta\alpha$ for $\Lambda_{LE} = 65^\circ$ Cambered Wing, $n = 0.05$

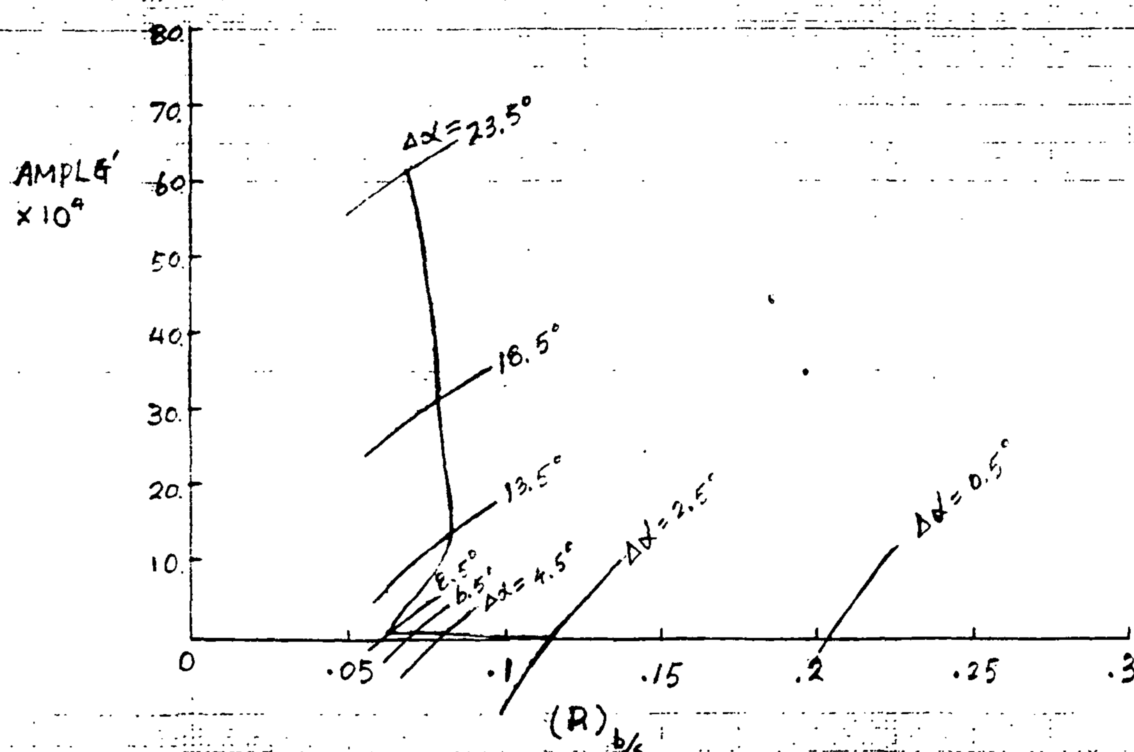

FIG 4. AMPLG′ VS. $(R)_{b/s}$ for $\Lambda_{LE} = 65^\circ$ Cambered Wing, $n = 0.05$.

ORIGINAL PAGE IS
OF POOR QUALITY

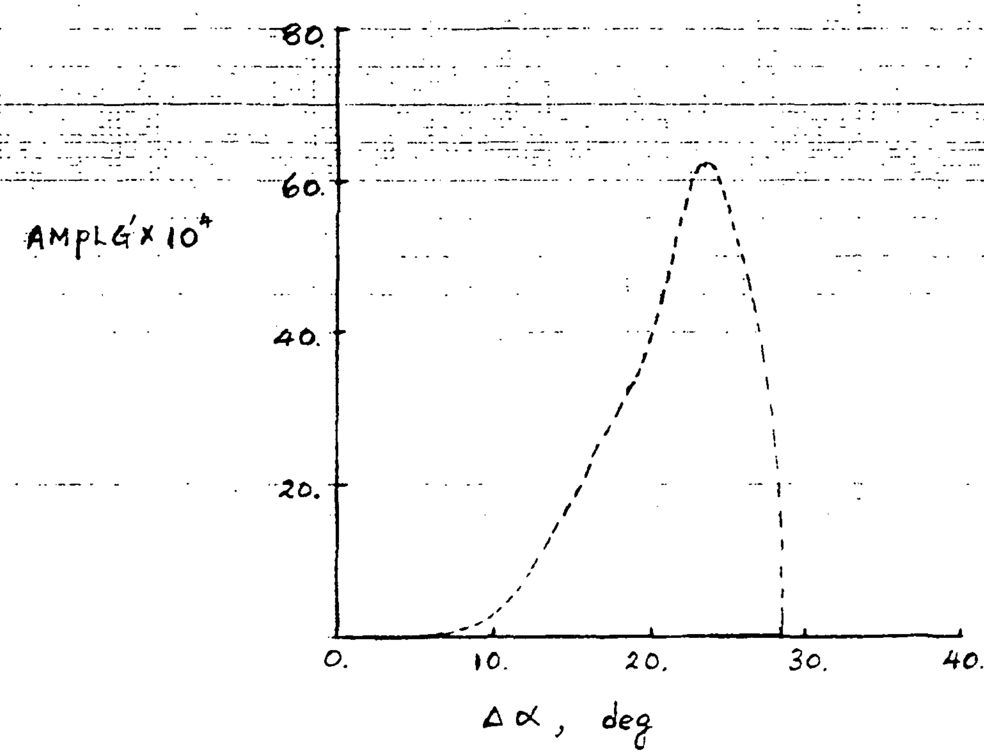

FIG 5. AMPLG' VS. Δα for a 65-deg. Flat Delta Wing, $\eta = 0.05$.

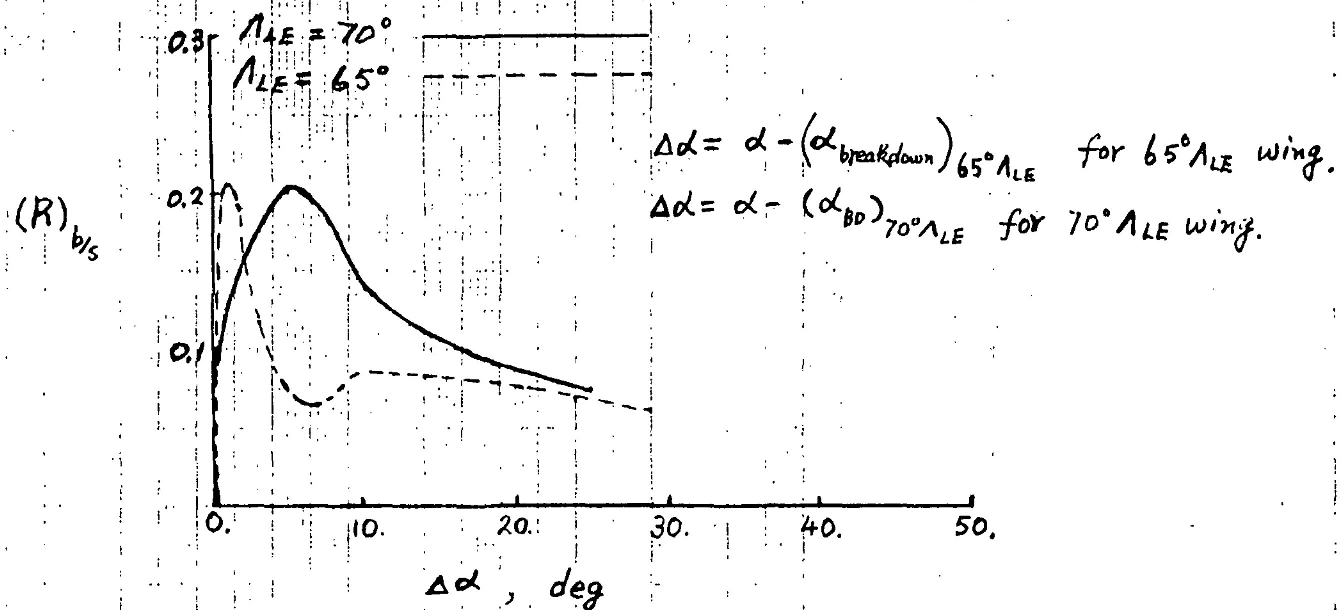

FIG 6. $(R)_{b/s}$ VS. $\Delta\alpha$ for $\Lambda_{LE} = 70°$ and $65°$ Cambered Wing. $n = 0.05$.

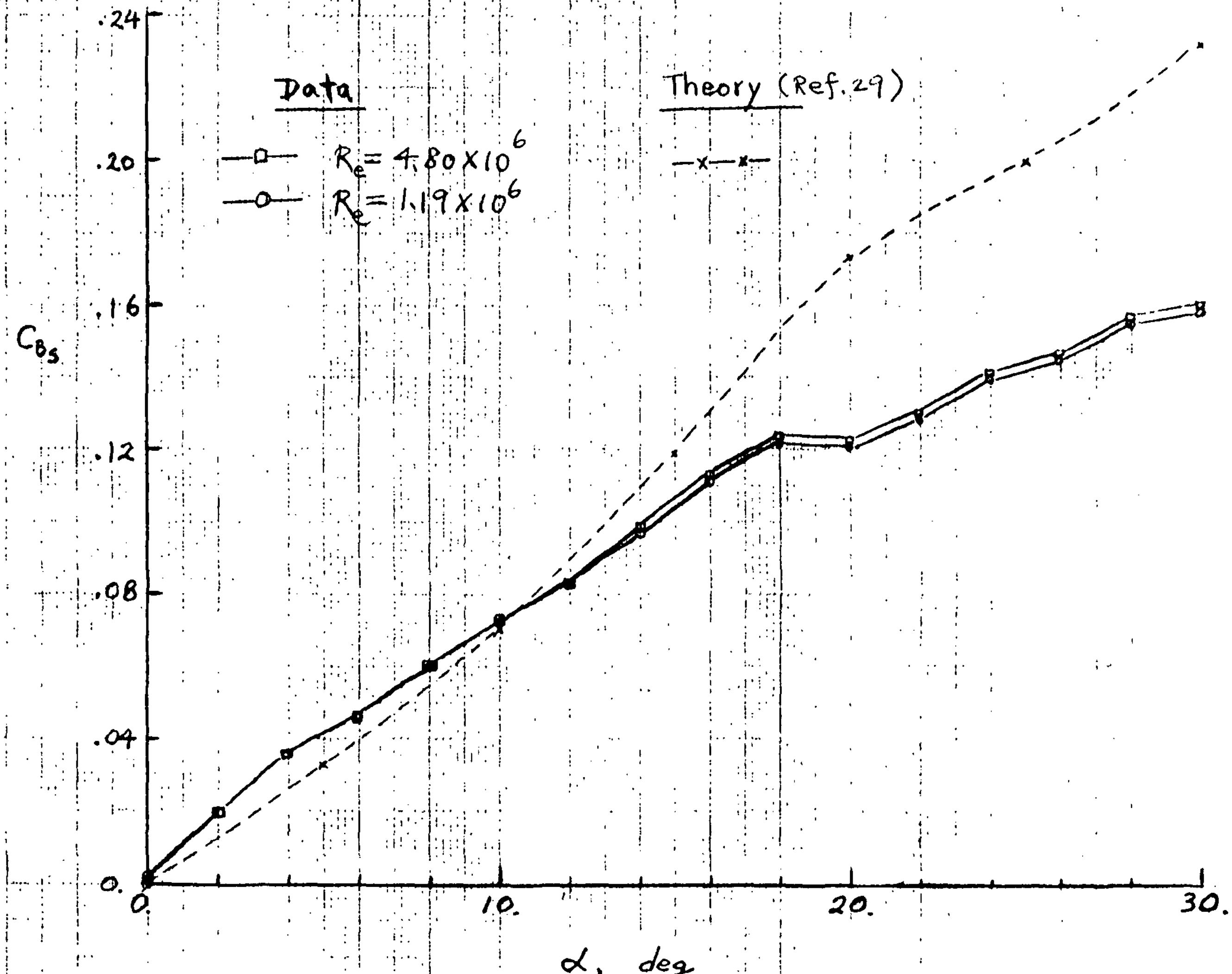

FIG 7. Steady Bending Moment Coeff C_{B_S} VS. α of $\Lambda_{LE} = 65°$ Flat Wing at $M = .35$

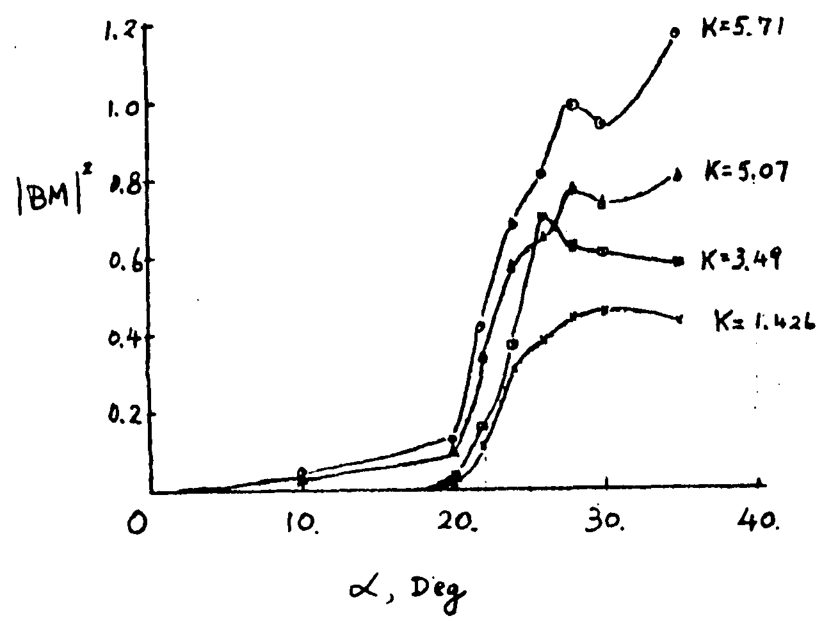

Fig 8. Power Spectral Density vs. α for Root Bending Moment of $\Lambda_{LE} = 65°$ Delta Wing.

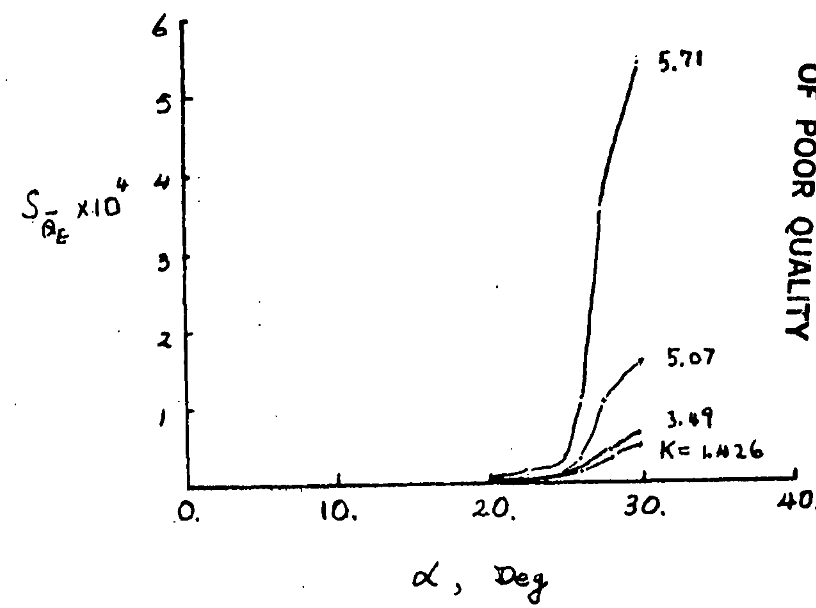

Fig 9. Plunging Amplitude Req'd Factor vs. α for $\Lambda_{LE} = 65°$ Delta Wing.

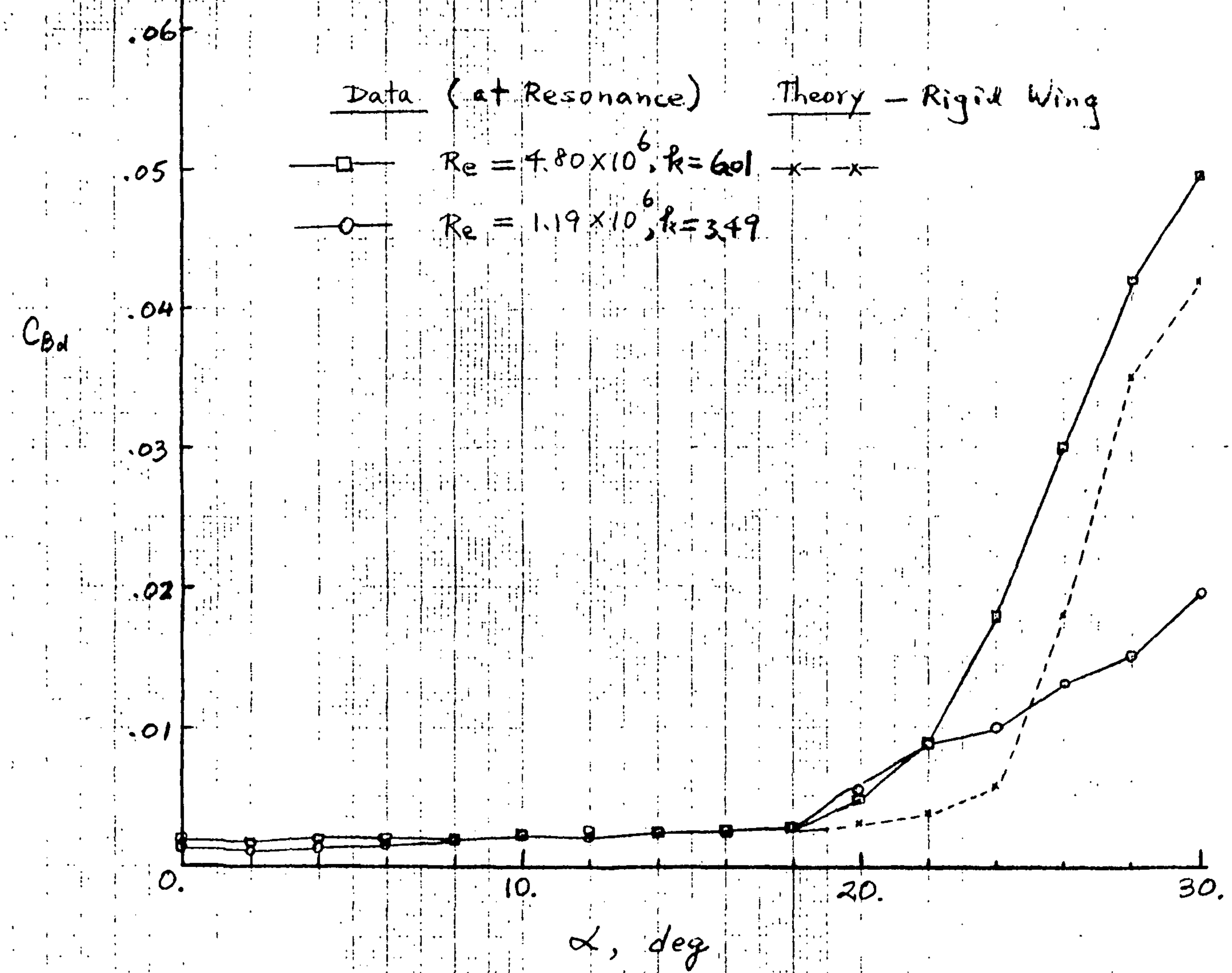

FIG 10. Dynamic Bending Moment Coeff C_{Bd} VS. α of $\Lambda_{LE} = 65°$ Flat Wing at $M = .35$

Appendix B:

Water Tunnel Testing of an F-18 Model

by

William H. Wentz, Jr.,

Wichita State University

DISK: S5 FILE:FA18/JA6

SUBJECT: PROGRESS REPORT, F/A-18 FIN BUFFET PROJECT

To: Eddie Lan, KU Date: 20 Jan 1986

From: Bill Wentz, WSU

STATUS OF WORK STATEMENT ITEMS:

The work statement items for the WSU portion of this project are quoted from the proposal, followed by the status for each item.

1. "Participate in detailed water tunnel test planning with NASA-Dryden and Navy personnel."- Planning and tests were completed during December 1985.

2. "Assist in the interpretation of available literature on F-18 and similar aircraft pertinent to the fin buffet problem."- This activity is to be in coordination with Professor Lan. No activity to date on this task.

3. "Review data obtained from water tunnel tests."- This has been a continuing process since completion of the tests. Key results are included in later sections of this report. At the present time, no additional water tunnel tests are recommended. Possible recommendations for addtitional water tunnel tests, and recommendations for the flight tests will follow completion of analysis of water tunnel test data.

4. "Contribute to the preparation of a technical report summarizing the results of this project."- Water tunnel test results are being prepared in form appropriate for the final report.

FACILITY AND MODELS:

Water Tunnel tests were conducted in the NASA-Dryden flow facility during the period 13-17 Dec 1985. Model configurations were as follows:

Basic F/A-18. - This model is essentially the complete aircraft configuration with missiles removed. Wing leading edge flaps were deflected 34^o and trailing edge flaps were un-deflected. This configuration is consistent with flight operations at angles of attack above 25^o.

F/A-18 without wings. - This model was used to evaluate the interference effects of the wing and leading edge extension (LEX) flow fields.

F/A-18 without fins. - This model was used to evaluate the possibility that the fin "blockage" might generate an adverse pressure field of sufficient strength to cause premature bursting of the leading edge vortices.

F/A-18 without LEX's. - The purpose of this model was to identify the role and interaction of forebody vortices, and to ascertain possible wing or forebody vortex interactions with the fin.

All models were constructed from 1/48 scale commercially available Monogram kits, fitted with hypodermic tubing for introduction of flow tracers. The models were also equipped with engine exhaust tubing connected internally to the engine inlets so that engine inlet flow was simulated.

TEST CONDITIONS:

For all but a few tests, inlet flow was established to provide an inlet capture area ratio of one. Most tests were conducted at a tunnel speed of 0.25 ft/sec, which corresponds to a Reynolds number of 4,000 based on (1/48 scale) model wing mean aerodynamic chord of 0.24 ft. Mach number for this speed is 5×10^{-7}.

Angle of attack was varied from 0^{o} to 40^{o}, in 5^{o} increments. At 40^{o}, the model nose was nearly in contact with the test section wall, so higher angles could not be tested without use of an offset sting. Video and still photos were obtained from top and side views in separate runs. One series of runs were made with the basic configuration with 5^{o} sideslip.

INSTRUMENTATION:

Instrumentation consisted of video cassette recording equipment, and camera for still photos. In addition, the fin of the basic model was fitted with a strain-gage and 2 different types of surface hot-film anemometers (Disa and Micro-Measurements). These instruments were intended to detect unsteady flow over the fin, for correlation of fin buffet with flight test data. An oscilloscope was available for monitoring of strain-gage or hot-film output signals, and a modal analyzer was utilized to perform frequency analysis of the dynamic signals.

The Disa hot-film anemometer and the strain-gage provided only very low-level signals, and did not provide consistent results which could be distinguished from random noise. The MM hot film gage, however, produced a signal which displayed characteristics which changed in a consistent manner with angle of attack. Therefore only the data from this gage was utilized for spectral analysis.

RESULTS OF FLOW VISUALIZATION:

BASIC MODEL - The flow video and still pictures show a consistent and repeatable pattern for the vortex flow of this aircraft configuration. As angle of attack is increased from 0^{o}, increasingly stronger vortices form along the LEX's. These vortices flow aft above the horizontal tail surfaces but beneath the fins for angle below 20^{o}. At 20^{o}, busting occurs aft of the wing trailing edge and outboard and beneath the fin. At 25^{o} angle of attack, the LEX vortex burst point is located inboard, with the primary axis of rotation nearly coincident with the fin leading edge. The burst point is slightly forward from the fin leading-edge at this angle of attack. As angle of attack is increased further, the burst point progressively moves forward. Vortex burst locations are shown in figures 1 and 2.

MODEL WITHOUT FINS - The absence of the fins had little effect on the flow field. Vortex locations and burst position were essentially unchanged from the basic model.

MODEL WITHOUT WINGS - In this configuration, LEX vortices formed in much the same manner as for the full model. As angle of attack was increased, however, the vortices were located at more inboard location than the basic model, and they remained intact, without bursting, up to 30^{o} angle of attack. This test series clearly indicates that the wing pressure field has a dominant role in the vortex bursting process. The adverse pressure gradient field associated with the portion of the wing aft of the leading edge flap hingeline is evidently a dominant factor producing vortex bursting.

MODEL WITHOUT LEX'S - With this model, no clear picture of vortices impinging on the fins was observed. Comparison of this configuration with the basic model reveals the strong role of the LEX's in producing the vortices which impinge on the fins.

RESULTS OF HOT-FILM SIGNALS: (BASIC MODEL ONLY)

The modal analyzer was utilized to obtain Psd data for each angle of attack from 0^{o} to 40^{o}. Results of these studies are summarized as follows:

(1) For angles of attack of 0^{o} to 20^{o}, no dominant frequency was observed.

(2) For angles of attack of 25^{o}, 30^{o}, 35^{o} and 40^{o}, dominant frequencies were discernable.

For 30° and 35°, runs were also made with tunnel speeds of approximately two- and three-times the nominal value. Results were plotted as frequency versus velocity in figures 3 through 6. These results show that frequency increases linearly with tunnel speed, resulting in a constant Strouhal number. Further, the Strouhal number associated with the vortex bursting is essentially independent of angle of attack. The observed Strouhal number is approximately 0.7 for all cases.

All test conditions scheduled have been run, and all video cassettes, photos and modal analyzer plots have been provided to WSU.

CURRENT ACTIVITIES: The NASA-provided video 3/4-inch tape cassettes have been transcribed onto 1/2-inch tape cassettes for ease of analysis using the WSU stop-action VCR unit. Analysis of these tapes is continuing, and WSU will extract primary LEX vortex location (vortex core location and location of the bursting point) from these images for the sideslip and non-standard configuration cases. Additional narrative describing the flow phenomena and associated hot film measurements will be developed.

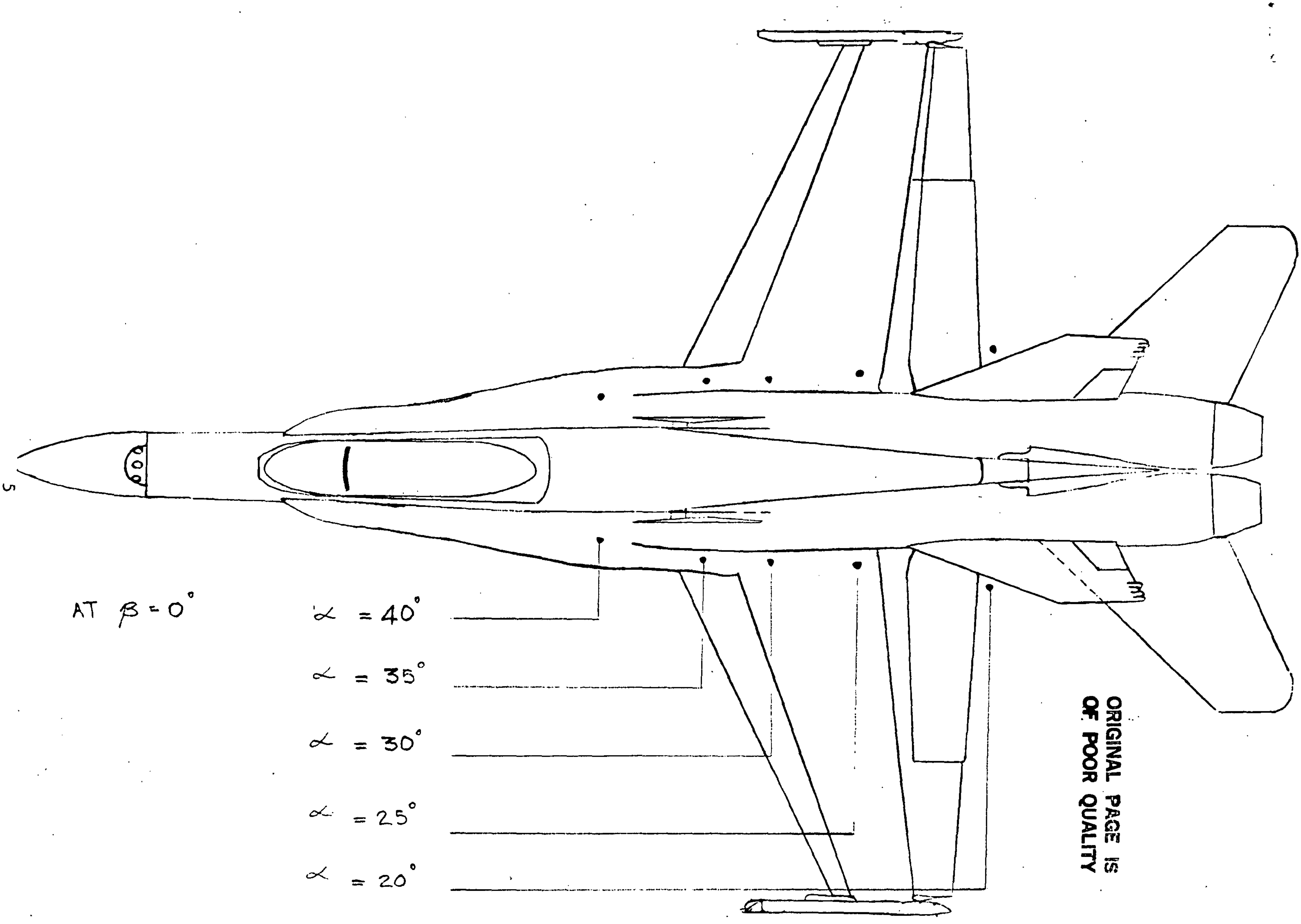

FIGURE 1 — VORTEX BREAKDOWN LOCATIONS – HORIZONTAL PLANE

P.P. 1/16/86

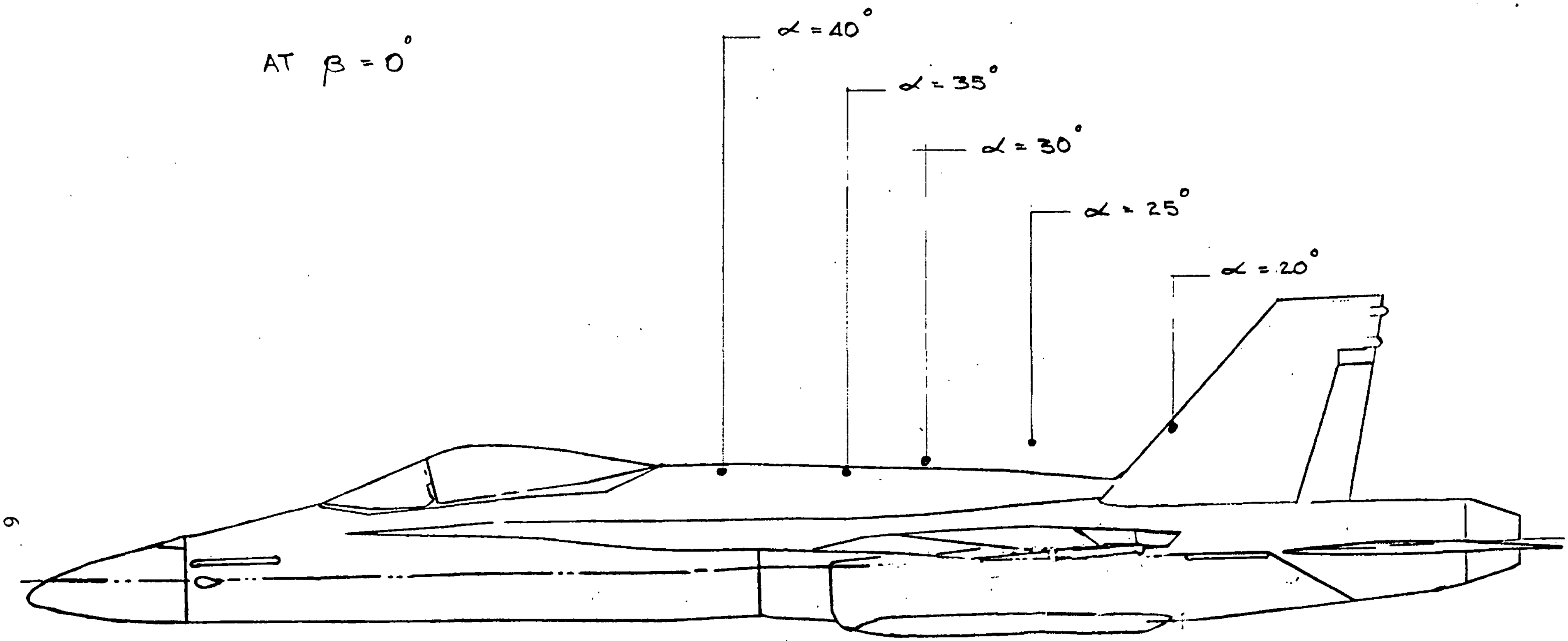

FIGURE 2 - VORTEX BREAKDOWN LOCATIONS - VERTICAL PLANE

P.P. 1/16/86

ORIGINAL PAGE IS OF POOR QUALITY

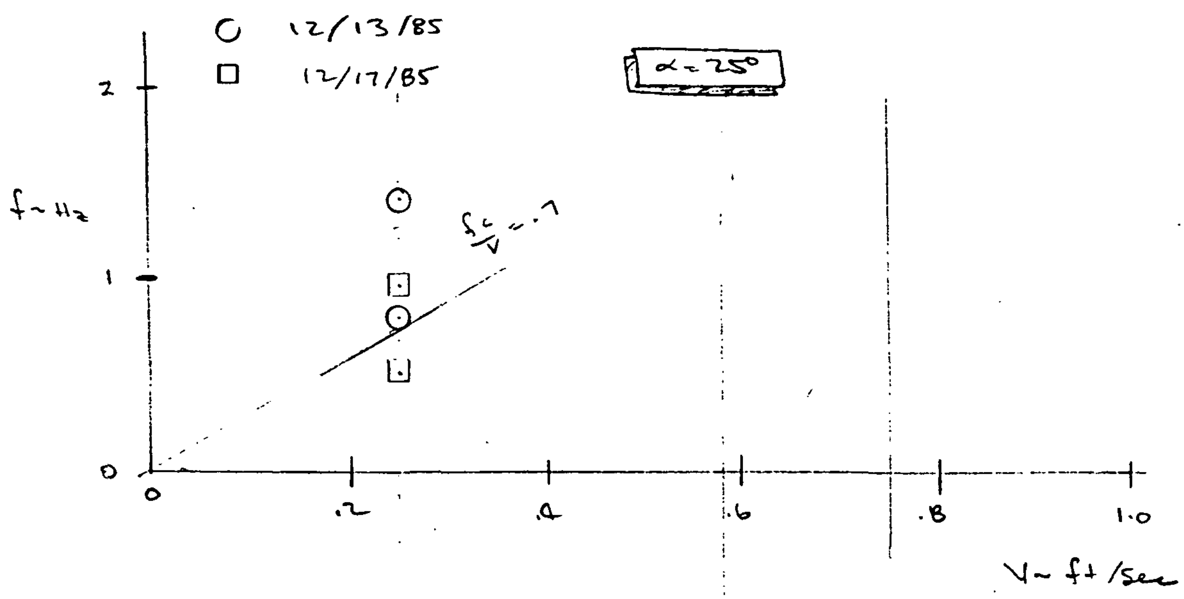

FIGURE 3 - BUFFET FREQUENCY, α = 25°

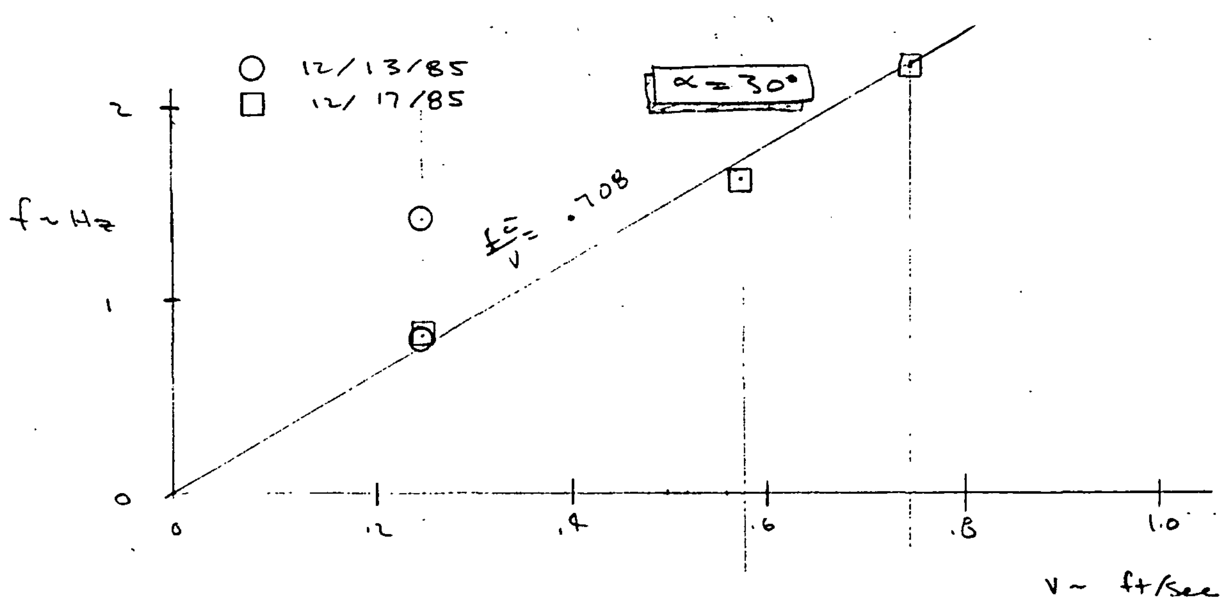

FIGURE 4 - BUFFET FREQUENCY, α = 30°

ORIGINAL PAGE IS
OF POOR QUALITY

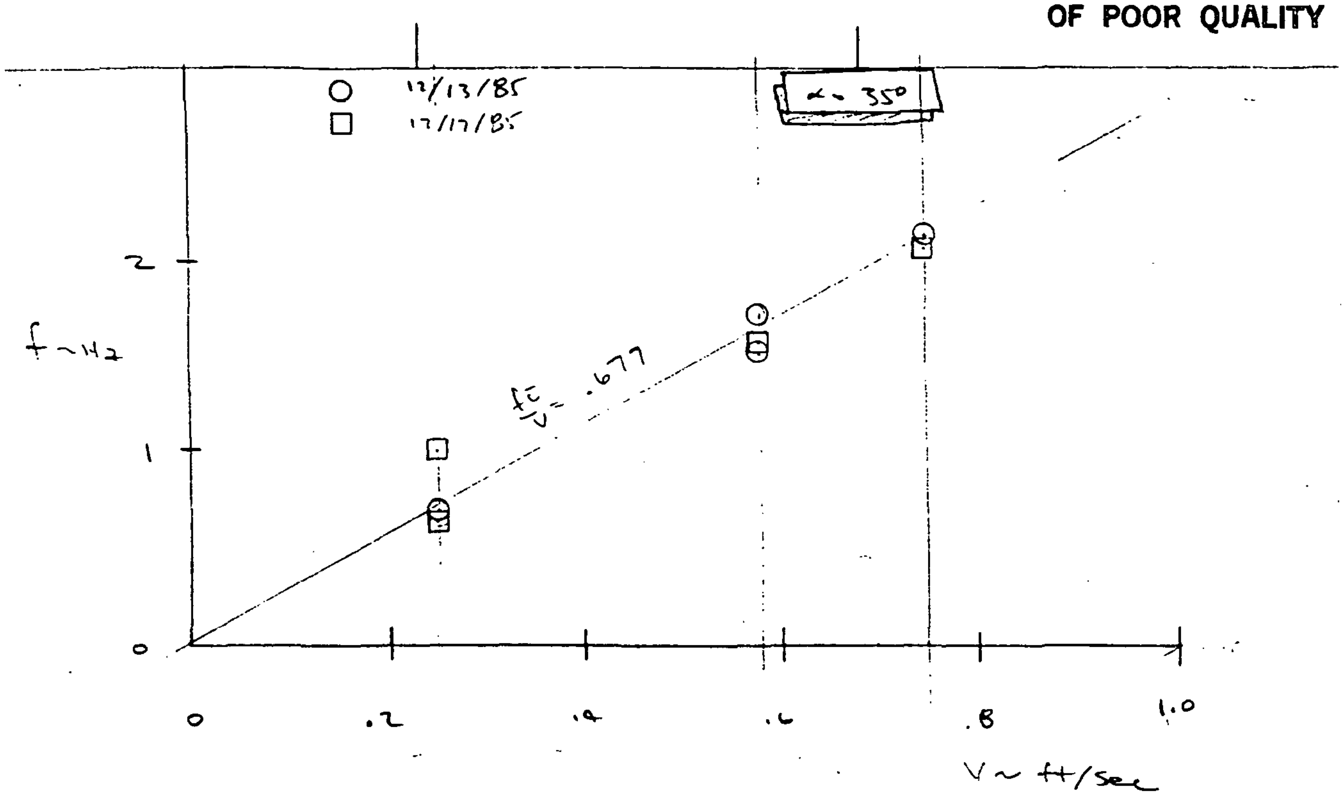

FIGURE 5 - BUFFET FREQUENCY, α = 35°

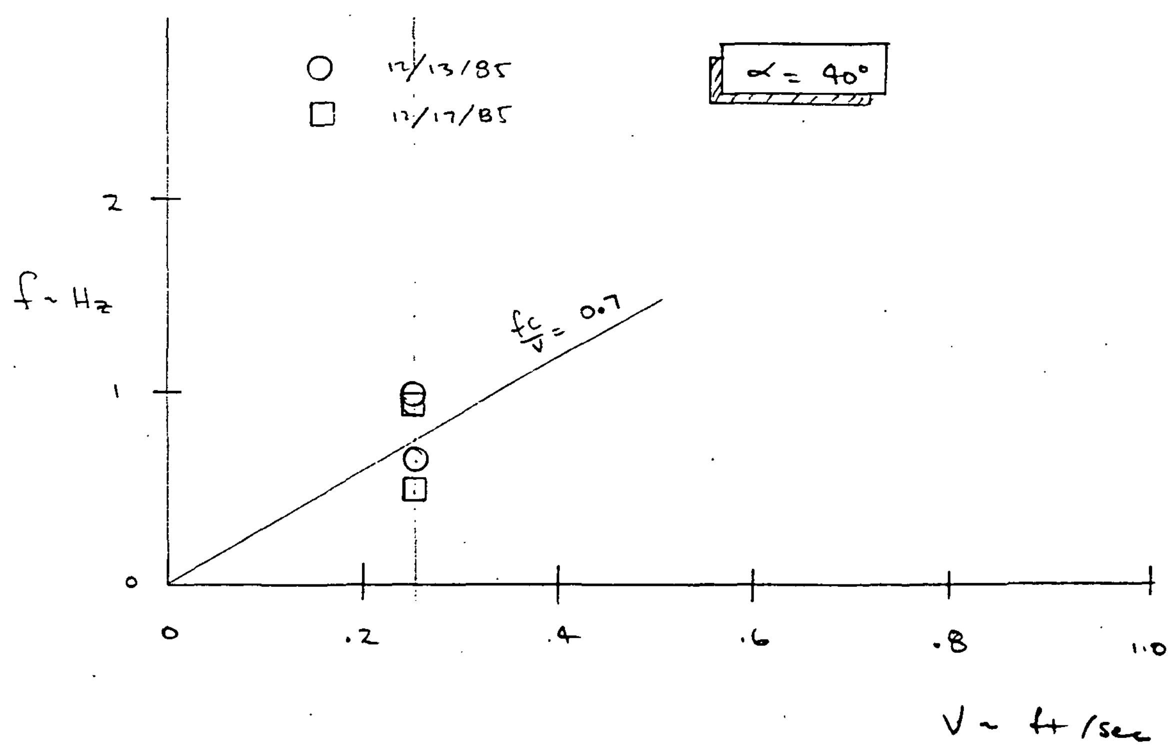

FIGURE 6 - BUFFET FREQUENCY, α = 40°